Release of Magnetic Nanoparticles from Cell-Encapsulating Biodegradable Nanobiomaterials

Feng Xu,[†,#] Fatih Inci,[†] Omer Mullick,[†] Umut Atakan Gurkan,[†] Yuree Sung,[†] Doga Kavaz,[†] Baoqiang Li,[†] Emir Baki Denkbas,[‡] and Utkan Demirci[†,§,*]

[†]Demirci Bio-Acoustic-MEMS in Medicine (BAMM) Laboratory, Center for Biomedical Engineering, Department of Medicine, Brigham and Women's Hospital, Harvard Medical School, Boston, Massachusetts 02139, United States , [‡]Nanotechnology and Nanomedicine Division, The Institute for Graduate Studies in Science and Engineering, Hacettepe University, 06800, Ankara, Turkey, [§]Harvard—MIT Health Sciences and Technology, Cambridge, Massachusetts 02139, United States. [#]Current address: The Key Laboratory of Biomedical Information Engineering of Ministry of Education, School of Life Science and Technology, Xi'an Jiaotong University, Xi'an 710049, China, and Biomedical Engineering & Biomechanics Center, Xi'an Jiaotong University, Xi'an 710049, P.R. China.

ABSTRACT The future of tissue engineering requires development of intelligent biomaterials using nanoparticles. Magnetic nanoparticles (MNPs) have several applications in biology and medicine; one example is Food and Drug Administration (FDA)-approved contrast agents in magnetic resonance imaging. Recently, MNPs have been encapsulated within cell-encapsulating hydrogels to create novel nanobiomaterials (*i.e.*, M-gels), which can be manipulated and assembled in magnetic fields. The M-gels can be used as building blocks for bottom-up tissue engineering to create 3D tissue constructs. For tissue engineering applications of M-gels, it is essential to study the release of encapsulated MNPs from the hydrogel polymer network and the effect of MNPs on hydrogel properties, including mechanical characteristics, porosity, swelling behavior, and cellular response (*e.g.*, viability, growth). Therefore, we evaluated the release of MNPs from photocrosslinkable gelatin methacrylate hydrogels as the polymer network undergoes biodegradation using inductively coupled plasma atomic emission spectroscopy. MNP release correlated linearly with hydrogel biodegradation rate with correlation factors (Pearson product moment correlation coefficient) of 0.96 ± 0.03 and 0.99 ± 0.01 for MNP concentrations of 1% and 5%, respectively. We also evaluated the effect of MNPs on hydrogel mechanical properties, porosity, and swelling behavior, as well as cell viability and growth in MNP-encapsulating hydrogels. Fibroblasts encapsulated with MNPs in hydrogels remained viable (>80% at $t = 144$ h) and formed microtissue constructs in culture ($t = 144$ h). These results indicated that MNP-encapsulating hydrogels show promise as intelligent nanobiomaterials, with great potential to impact broad areas of bioengineering, including tissue engineering, regenerative medicine, and pharmaceutical applications.

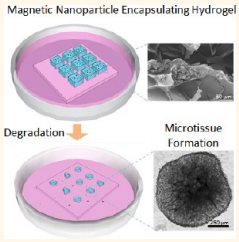

KEYWORDS: magnetic nanoparticles · nanoparticle release · hydrogel degradation · nanotoxicity · intelligent nanobiomaterials

The recent convergence of biomaterials and nanotechnology has enabled the development of intelligent nanobiomaterials, such as nanoparticle-encapsulating hydrogels for applications in tissue engineering and regenerative medicine.[1−3] These nanobiomaterials provide unique properties to address challenges in biology, medicine, and materials science,[4−6] *e.g.*, modifiable mechanical and interfacial properties of a nanoscaffold to mimic native extracellular matrix (ECM).[7] Due to their innate magnetic characteristics and biocompatibility, magnetic nanoparticles (MNPs) have been widely used in biomedical applications, such as cell patterning, three-dimensional (3D) cell culture, targeted drug/gene delivery, clinical imaging, and biosensors for *in vivo* biomarker detection.[8−17] Further, MNPs have been integrated with hydrogels *via* microfluidics,[18−20] for example, to form multiplexed bioassays[21,22] and to generate scaffolds for on-demand drug and cell delivery.[23] Recently, MNPs (specifically iron oxide nanoparticles) have been encapsulated in microscale hydrogels to fabricate novel nanobiomaterials (M-gels). These materials can be fabricated as microscale building blocks and manipulated under controlled magnetic fields to create tissue constructs using bottom-up tissue engineering approaches.[24,25] The magnetic approach using these M-gels has potential to broadly impact multiple fields including bioengineering, tissue engineering, and pharmaceutical applications.

The U.S. Food and Drug Administration (FDA) has approved the use of MNPs in several applications such as imaging agents,[26] and tolerability of mammalian cells to MNPs has been demonstrated under used conditions.[27,28] It is notable that FDA-approved nanoparticles are smaller in size than the MNPs previously discussed. They are equally responsive to magnetic fields, and they are relatively easier to remove from the body.[29] MNPs can be introduced to a microenvironment along with ECM and/or cells. In these applications, MNPs should not remain within the assembled

* Address correspondence to udemirci@rics.bwh.harvard.edu.

Received for review February 29, 2012 and accepted June 9, 2012.

Published online June 10, 2012
10.1021/nn300902w

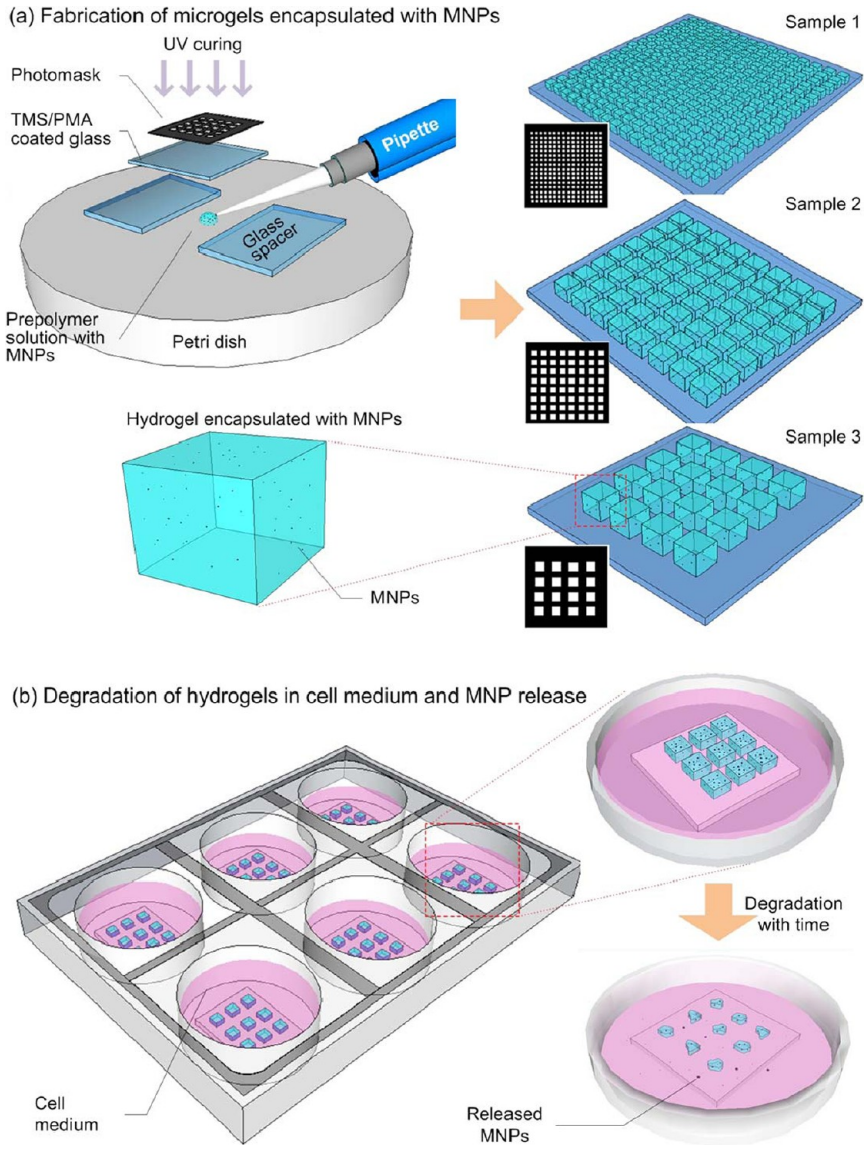

Figure 1. Schematic of magnetic nanoparticle (MNP) encapsulation and release from hydrogels. (a) Fabrication of cell encapsulating hydrogels with MNPs. Prepolymer solution (250 μL) was pipetted onto a Petri dish surface, and then, exposed to 6.9 mW/cm^2 UV for 40 s. Three hydrogel samples of sizes with matched total volumes were fabricated. Sample 1 consisted of an array of 256 hydrogels, each with dimensions of 500 μm $\times$ 500 μm $\times$ 300 μm. Sample 2 consisted of an array of 64 hydrogels, each with dimensions of 1 mm $\times$ 1 mm $\times$ 300 μm. Sample 3 consisted of an array of 16 hydrogels, each with dimensions of 2 mm $\times$ 2 mm $\times$ 300 μm. All samples were cultured in 4 mL of 3T3 media, with or without the addition of 2 U/mL collagenase type I. (b) Degradation of hydrogels and release of encapsulated MNPs. As the hydrogels degraded, encapsulated MNPs were released into the media. Media was collected at intervals of 6 h, and corresponding MNP concentration was tested using inductively coupled plasma atomic emission spectroscopy (ICP-AES).

constructs and should be released as the gels biodegrade,[30,31] and cells secrete their own ECM. Although MNPs are used clinically, further studies on the release of magnetic nanoparticles from biomimetic composite materials and their effects on mechanical gel characteristics, swelling behavior, porosity, and cell viability and growth are needed for successful applications in tissue engineering.[32]

In this paper, we report the release of MNPs encapsulated in methacrylated gelatin (GelMA) hydrogels as the hydrogels undergo degradation in the presence of 3T3 cells *in vitro*. We assessed the effects of encapsulated MNPs on cell viability and proliferation and evaluated the mechanical properties, swelling behavior, and porosity of MNP-encapsulating microgels.

RESULTS AND DISCUSSION

We fabricated M-gels of different sizes and performed biodegradation assays (Figure 1). To evaluate the effect of MNP encapsulation on mechanical properties of M-gels, mechanical testing (nonconfined compression analysis) was performed on GelMA hydrogels (control) and MNP (1% and 5%)-encapsulating GelMA hydrogels (Figure 2). Compression analysis was performed until the hydrogels were structurally

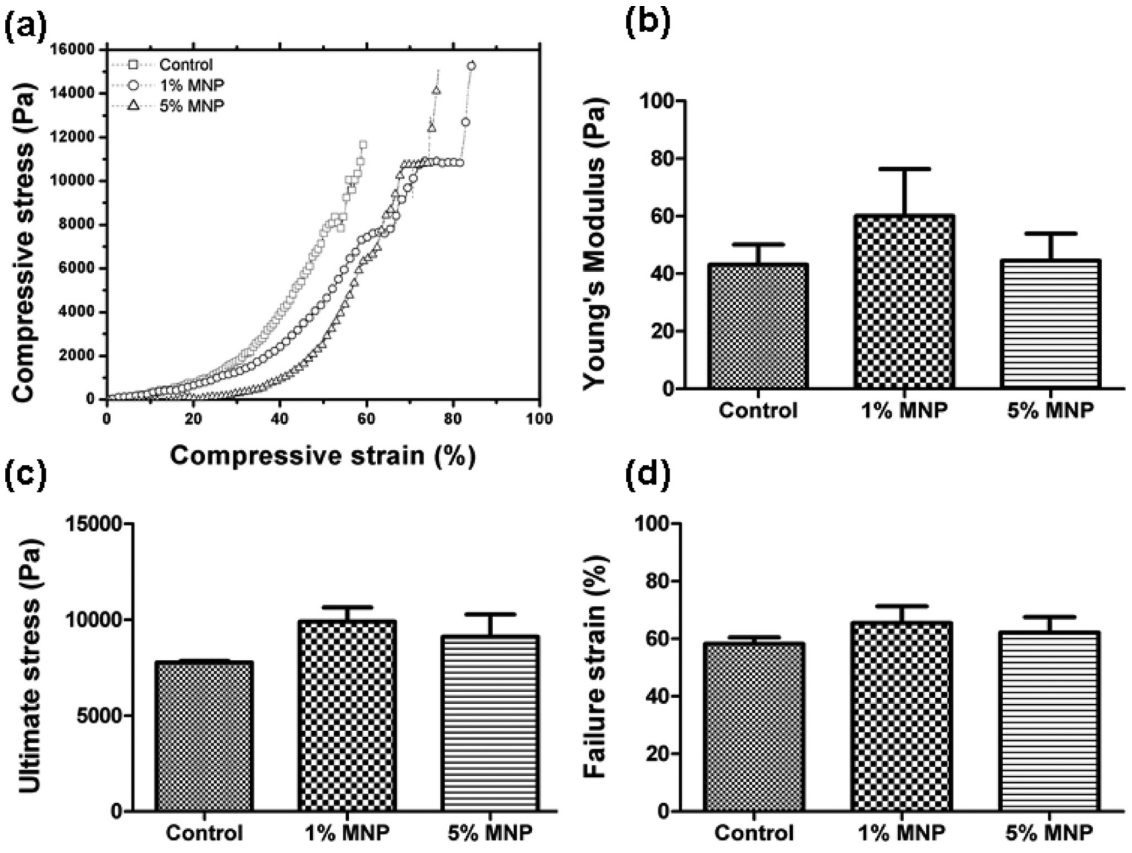

Figure 2. Mechanical properties of control and MNP-encapsulating (1% and 5%) hydrogels. (a) Representative stress−strain curves were plotted from nonconfined compression tests for control and MNP (1% and 5%)-encapsulating hydrogels. (b) Young's modulus was measured by calculating the slope in the initial linear region (5−20%) of the compression analysis. (c) Ultimate stress and (d) failure strain were calculated using data from nonconfined compression tests. Mechanical properties were statistically comparable for control and MNP-encapsulating (1% and 5%) hydrogels. Statistical analyses were performed by using analysis of variance (ANOVA) with Tukey's *posthoc* test for multiple comparisons ($n = 5$, $p < 0.05$). Data are presented as average ± standard error of the mean.

deformed, and failure strength was recorded (Figure 2A). Young's modulus (Figure 2B) was measured by determining the slope of the initial linear region of the stress−strain curve (Figure 2A). There was no statistically significant difference between these samples ($p > 0.05$). We further analyzed the ultimate stress (Figure 2C) and failure strain (Figure 2D) of hydrogels. These analyses showed comparable results in ultimate and failure strain levels for control and MNP-encapsulating hydrogels.

To quantify the degradation of hydrogel samples, we measured the area change of hydrogels of three different sizes as a function of culture time for MNP concentrations of 1% (Figure 3A, S1A) and 5% (Figures 3B, S1B), with constant cross-linking settings. We observed that the smaller hydrogels (500 μm × 500 μm × 300 μm) degraded at a much higher rate than the larger hydrogels of size 1 mm × 1 mm × 300 μm and 2 mm × 2 mm × 300 μm that had similar degradation rates. For instance, for 1% MNP concentration at $t = 30$ h, full degradation was observed for 500 μm hydrogels, while 1 and 2 mm hydrogels experienced 71.8 ± 29.2% and 86.4 ± 17.8% degradation, respectively (Figure 3A). Further, we observed that hydrogels fabricated using 5% MNP prepolymer solution degraded at a much faster rate than the 1% MNP hydrogels. At $t = 24$ h, 5% MNP hydrogels were completely degraded (Figure 3B), while the comparable 1% MNP gels remained partially degraded at this time period (Figure 3A).

To further evaluate hydrogel degradation, we measured the dry weight of hydrogels at different time points during gel degradation using collagenase type I (Figure 3C). The degradation based on mass change was observed to be comparable to the degradation based on area change (Figure 3A, B). We observed that cell-encapsulating hydrogels degraded at a much higher rate than cell-free hydrogels (Figure 3C). For instance, two groups of hydrogels encapsulating cells (with or without MNPs) completely degraded at $t =$ 72 h, while ~70% of the control hydrogels remained non-degraded at that time point. The presence of cells resulted in more than a 2-fold increase in hydrogel degradation rate (~48 h) as compared to cell-free hydrogels based on the time point (Figure 3C). Many naturally forming gels, such as collagen, hyaluronic acid, chondroitin sulfate, fibrin, and gelatin, have specific amino acid sequences that are recognizable by

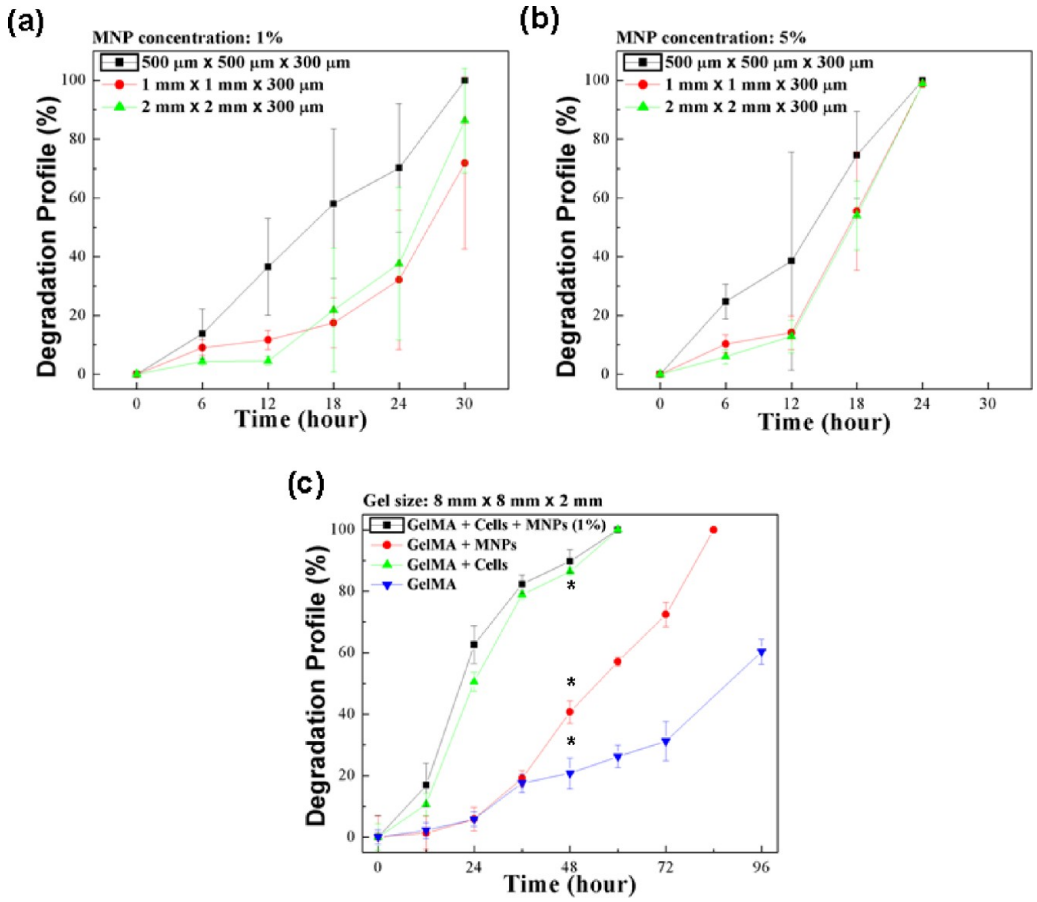

Figure 3. Evaluation of degradation profile of hydrogels cultured in 2 U/mL collagenase type I. (a) Degradation profile of 1% MNP-encapsulating hydrogels over time was measured using NIH ImageJ. (b) Degradation profile of 5% MNP-encapsulating hydrogels over time was measured using NIH ImageJ. (c) Degradation profile for 4 sets of 8 mm × 8 mm × 2 mm hydrogels was evaluated. Dry weight of the hydrogels was measured at 24 h intervals, and weight loss was determined as a function of time. *Significantly different according to ANOVA test with $p < 0.05$ ($n = 3-10$). Data are presented as average ± standard deviation.

cells. These specific sequences can be degraded by the cell-secreted enzymes at neutral pH.[33,34] It has been reported that the presence of cells accelerates degradation of alginate hydrogels.[35] The hydrogel degradation process has been shown to be promoted by cell growth, therefore, this process significantly depends on the presence of encapsulated cells. Additionally, the MNP-encapsulating hydrogels degraded to 70% of their original weight at $t = 72$ h, while the control hydrogel experienced 30% degradation in the same time period. The introduction of MNPs within the hydrogel matrix (~48 h) increased the hydrogel degradation by 1.5 times as compared to control (~96 h) based on the time point. These results indicated that the presence of both cells and MNPs increased the hydrogel degradation rate, as confirmed by the statistical analysis (Figure 3C). The observed degradation results may be attributed to altered structural properties of microgels due to the encapsulation of nanoparticles within the GelMA polymer matrix.

To evaluate the effect of encapsulated MNPs on hydrogel microstructure, we performed scanning electron microscope (SEM) imaging of the cross sectional area of control samples without MNPs and hydrogels with 1% and 5% MNPs (Figure 4A). We observed that there was a difference in hydrogel microstructure between MNP-encapsulating hydrogels and controls, where MNPs were located in hydrogel pores (Figure 4A). In the literature, dependence of a volume fraction of inorganic nanoparticles (NPs) (*e.g.,* Au and ZnO) on the mechanical properties of polyelectrolyte microcapsules was reported.[36,37] The rapid degradation of 5% MNP gels compared to 1% MNP gels and controls can be attributed to the higher MNP concentration.

To quantitatively evaluate the porosity of hydrogels, we analyzed SEM images by using NIH ImageJ software (Figure 4B). We observed a statistically significant difference in porosity between controls and 5% MNP-containing samples. There was no statistical difference between the 1% and 5% MNP gel samples (Figure 4B). We also evaluated the swelling characteristics of hydrogels. The swelling of gels depends on both the pore size of the polymer network and the polymer−solvent interactions.[38] Swelling analysis on controls and MNP (1% and 5%)-encapsulating hydrogels indicated that there was a statistically significant decrease in swelling ratio of hydrogels with increasing MNP concentration (Figure 4C).

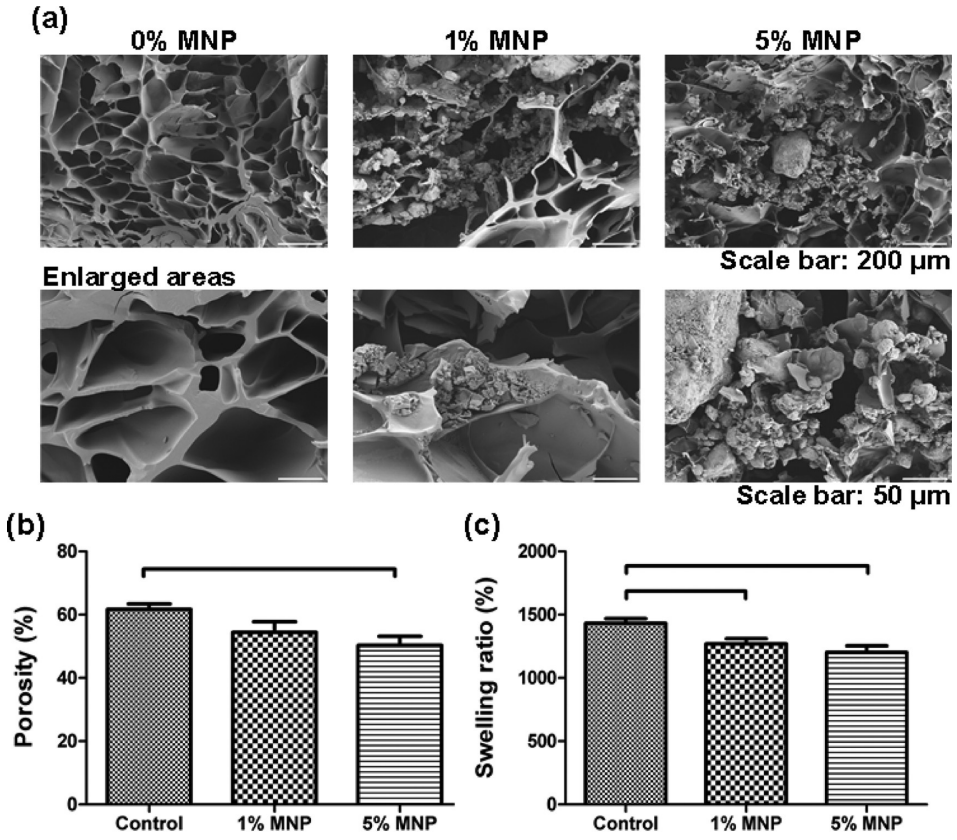

Figure 4. Scanning electron microscopy (SEM) images of cross-sections of control hydrogels and MNP (1% and 5%)-encapsulating hydrogels. (a) Three sets of 6 mm × 6 mm × 10 mm hydrogels were fabricated using photolithographic techniques. (b) The porosity analysis of control hydrogels and MNP (1% and 5%)-encapsulating hydrogels was performed by the NIH ImageJ software based on the SEM images. There was a statistically significant difference observed between the control and 5% MNP-encapsulating hydrogels. However, there was no statistically significant difference observed between the control and 1% MNP-encapsulating hydrogels. There was also no statistically significant difference observed between 1% and 5% MNP-containing hydrogels. Brackets connecting individual groups indicate statistically significant difference (analysis of variance (ANOVA) with Tukey's *posthoc* test for multiple comparisons, $n = 10-15$, $p < 0.05$). Data are presented as average ± standard error of the mean (SEM). (c) Swelling behavior is presented for control hydrogels and MNP-encapsulating (1% and 5%) hydrogels. There was a statistically significant difference between controls and MNP (1% and 5%)-encapsulating hydrogels. However, there was no significant difference between 1% and 5% MNP-encapsulating hydrogels. Brackets connecting individual groups indicate statistically significant difference (ANOVA with Tukey's *posthoc* test for multiple comparisons, $n = 16$, $p < 0.05$). Data are presented as average ± SEM.

The swelling ratio was significantly reduced ($p < 0.05$) when 1% or 5% MNP-encapsulating hydrogels were used. There was no significant difference ($p > 0.05$) in swelling characteristics between 1% and 5% MNP-encapsulating hydrogels (Figure 4C).

To investigate the effect of gel size on MNP release and its correlation with hydrogel degradation, we measured the MNP release by using inductively coupled plasma atomic emission spectroscopy (ICP-AES) (Figure 5) for three different hydrogel sample arrays corresponding to those used in the gel area change test (Figures 5, S2). We observed that the larger hydrogels (1 mm × 1 mm × 300 μm, 2 mm × 2 mm × 300 μm) encapsulated more MNPs than the smaller hydrogels (500 μm × 500 μm) and, hence, released more MNPs overall (Figure 5). On the other hand, there may be limitations on the maximum amplitude and duration of the local magnetic fields that can be used for 3D assembly. High levels of magnetically induced force may shear the gels and compromise the microgel integrity. Since low-intensity, short-duration magnetic fields from permanent magnets yield satisfactory assembly of these MNP-encapsulating microgels using permanent magnets[2], potential problems due to heating caused by alternating magnetic fields do not constitute a challenge. Since aggregation of MNPs is known to occur in prepolymer solutions,[39,40] there exists a possibility that the MNP distribution is not the same in each M-gel. MNPs may aggregate in prepolymer solutions, resulting in nonuniform MNP distributions in M-gels, which may affect the MNP release characteristics. Further, some M-gels could also have a lower affinity to the magnetic field. Hence, to minimize the occurrence of nonuniform MNP aggregation, we performed prefiltering and sonication during the M-gel fabrication process. The biodegradation of hydrogels will allow the release of the MNPs, which would then potentially lead to cleansing of the MNPs

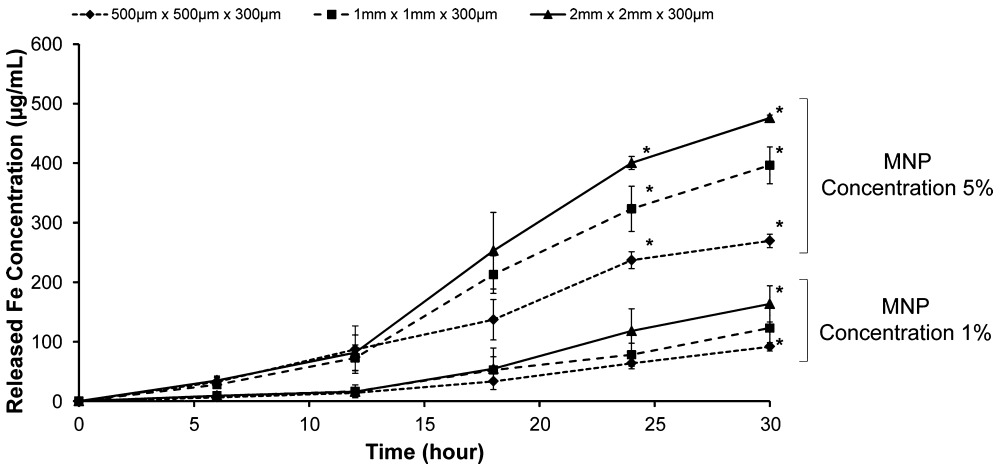

Figure 5. Release profile of MNPs during hydrogel degradation measured by inductively coupled plasma-atomic emission spectroscopy (ICP-AES). At 6 h intervals, 3T3 media surrounding the hydrogels was collected and iron (Fe) concentration was measured using ICP-AES. Hydrogels were fabricated using two different MNP concentrations (1% and 5%). In 1% MNP hydrogels, concentration of released MNPs was significantly different between 2 mm hydrogels and 500 μm hydrogels at t = 30 h. In 5% MNP hydrogels, concentration of released MNPs was significantly different between all three gel sizes at t = 24 and 30 h. *Significantly different according to ANOVA test with $p < 0.05$. Data are presented as average $\pm$ standard deviation.

from the tissue constructs *in vivo*. The fabrication of biodegradable hydrogels, which can be used as drug delivery systems or nanoparticle delivery systems, is one of the widely growing and promising areas in biomedicine (*e.g.,* tissue engineering) and material science.

We calculated the efficiency to encapsulate MNPs in hydrogels during gel fabrication for both 1% and 5% MNP hydrogels. An average efficiency of 20% was calculated for 5% MNP hydrogels. This result indicated that 5% MNP hydrogels encapsulated approximately three times more MNPs than the 1% MNP hydrogels, although results show that there was an average of five times more MNPs in the 5% MNP prepolymer solution. To assess the correlation between MNP release and hydrogel degradation, we statistically compared the surface area change of hydrogels (Figure 3A, B) with ICP-AES results (Figures 5, S2). The Pearson product moment correlation coefficients were 0.961 $\pm$ 0.03 and 0.990 $\pm$ 0.01 for 1% and 5% MNP concentrations, respectively (Figure S2). These results indicated that there was a strong linear correlation between MNP-encapsulating hydrogel degradation and release rates of encapsulated MNPs.

To ensure favorable biocompatibility, to minimize toxicity due to nanoparticles, and to ensure general applicability of the results, FDA-approved nanoparticles can be used. Approved MNPs used in MRI imaging, including superparamagnetic iron oxides (SPIO, ferumoxides) and ultrasmall SPIO (USPIO, ferumoxtran), can be potentially used for tissue engineering applications. To assess the effect of MNPs in cell-encapsulating hydrogels, we tested the short-term cell viability with collagenase type I at t = 6, 12, and 24 h (Figures 6A, S3A) and long-term cell viability without collagenase type I at t = 24, 48, 72, 96, 120, and 144 h (Figures 6B, S3B). In both short- and long-term cell viability experiments, we cultured 3T3 cells in the absence of hydrogels as a control. We observed that cell viability in both 1% and 5% MNP hydrogels was comparable to the MNP-free control in both short-term and long-term viability tests. We observed significant cell growth (fold changes for number of cells compared to 24 h of culture) in 1% and 5% MNP hydrogels. The fold changes in 1% and 5% MNP hydrogels were less than that observed in control hydrogels (Figure 6C). We also monitored cell proliferation in long-term cultures. To test the long-term cell viability and growth of 3T3 cells in MNP-encapsulated hydrogels, we fabricated cell encapsulating hydrogels (500 μm $\times$ 500 μm $\times$ 300 μm in size) and cultured them. These cell-encapsulating hydrogels were imaged at time points t = 1, 72, 108, and 144 h and showed both cell proliferation and cell growth (Figure 6D, S3B). The cells proliferated in the MNP-encapsulating hydrogels and formed microtissue constructs after 144 h of culture. We noticed that the long-term cell culture displayed a similar degradation pattern to the enzyme-mediated degradation (Figure 3A, B).

Due to the widespread applications of nanoparticles in polymers,[41] several studies have been performed on nanoparticle release from a polymer matrix (*e.g.*, airborne release of nanoparticles[42−45]). Verberg *et al.* mathematically modeled the release of nanoparticles from microcapsules moving within a microchannel.[46] Their results indicated that the capsule elasticity and adhesion to the microfluidic channel walls significantly influenced nanoparticle release, which may be due to the change in surface energy of the capsule. Recently, release of nanoparticles from a biocompatible polymer matrix (*e.g.*, hydrogels) has been studied. It has been shown that the release of nanoparticles depends on several parameters including mechanical properties[47,48]

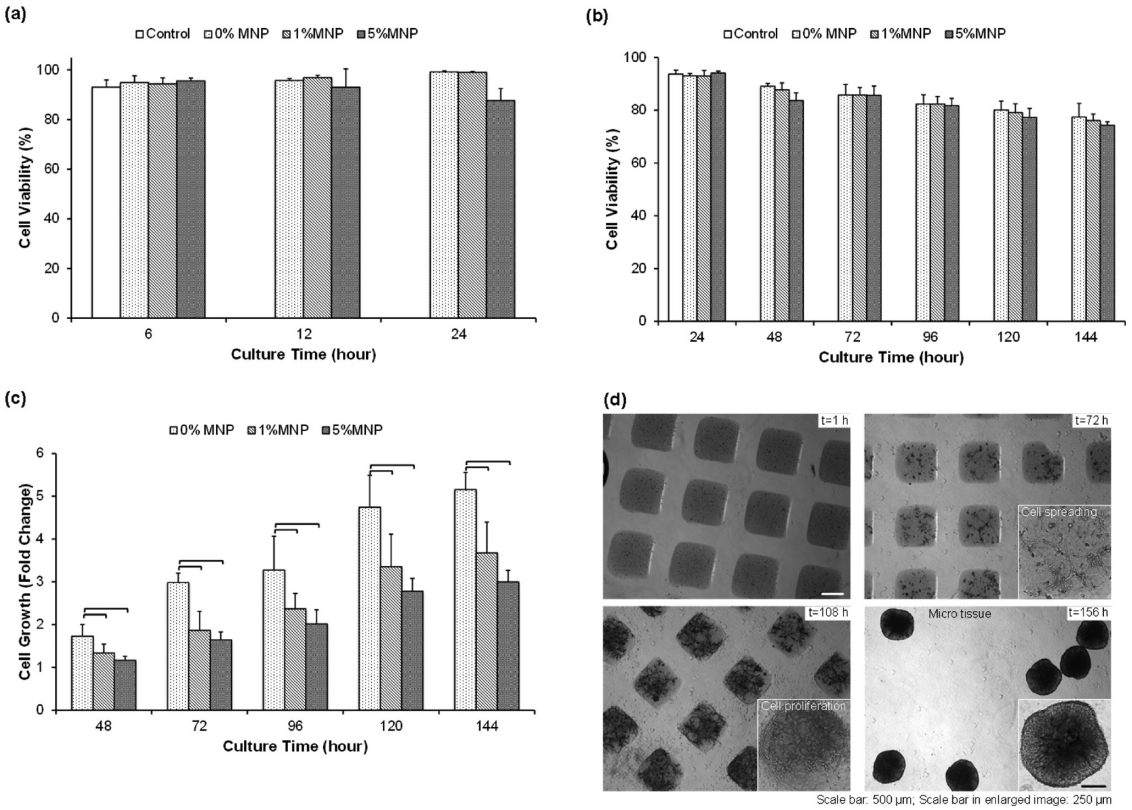

Figure 6. Cell growth in MNP-encapsulating hydrogels. (a) Short-term viability of NIH 3T3 fibroblasts cultured in 1% and 5% MNP hydrogels (1 mm × 1 mm × 300 μm) as a function of time (t = 6, 12, 24 h) as compared to MNP-free controls. 3T3 cells in the absence of hydrogel were cultured as controls. (b) Long-term viability of 3T3 cells in 1% and 5% MNP hydrogels as a function of time (t = 24, 48, 72, 96, 120, 144 h) was compared to MNP-free controls. 3T3 cells in the absence of hydrogels were cultured as controls. (c) Relative fold increase in growth of 3T3 cells in hydrogels with 1% and 5% MNP hydrogels as a function of time as compared to 24 h of culture. The presence of MNPs, regardless of concentration, affected cell growth. *Significantly different according to ANOVA test with $p < 0.05$ (n = 6). (d) Long-term culture of 3T3 cells with MNPs in 500 μm hydrogels. We observed cell proliferation and formation of microtissue constructs in the presence of MNPs. Data are presented as average ± standard deviation.

and hydrogel degradation. Release of polystyrene nanobeads immobilized in PEG-acrylate hydrogels was proportional to the enzyme concentration (*i.e.*, proteinase) secreted by cells encapsulated in hydrogels.[49] Although these studies elucidated some features of nanoparticle release from a polymer matrix, no study has yet evaluated the release of MNPs from hydrogels. This study evaluated the MNP release from hydrogels, and the results indicated the potential of MNP-based nanobiomaterials in biomedical applications.

CONCLUSIONS

In this study, we presented the progression of MNP-encapsulating hydrogel degradation and corresponding MNP release from cell-encapsulating hydrogels. The results indicated that the rate of hydrogel degradation increased in the presence of MNPs and cells encapsulated in hydrogels. There was a linear correlation between MNP release and degradation rates, suggesting effective release of MNPs during biodegradation. The cells encapsulated in hydrogels remained viable in the presence of MNPs and formed microtissue constructs in culture. Mechanical properties of MNP-encapsulating and control hydrogels were analyzed, and no significant differences were observed between the control and 1% and 5% MNP encapsulating hydrogel variants. When manipulated with magnetic fields, these hydrogels afford a high degree of spatial control, providing exciting opportunities in the creation of complex, cell-encapsulating 3D scaffolds. MNP-encapsulating hydrogels constitute a new type of hybrid nanobiomaterial that has potential to impact broad fields including tissue engineering, regenerative medicine, and drug delivery.

MATERIALS AND METHODS

Materials. In this study, photoinitiator 2-hydroxy-1-[4-(hydroxyethoxy)phenyl]-2-methyl-L-propanone (Irgacure 2959) was purchased from Ciba Geigy (Dover, NJ, USA). The live/dead viability/cytotoxicity kit for mammalian cells was purchased from Invitrogen Corporation (Invitrogen, Carlsbad, CA, USA). Collagenase type I was purchased from Worthington Biochemical Corporation (Lakewood, NJ, USA). The Omnicure S2000 UV/Visible Spot Curing System from EXPO Photonic Inc. (Mississauga, Ontario, Canada)

was used to polymerize the hydrogels. The MNPs were purchased as dry iron(II,III) oxide nanopowder (<50 nm; order #637106, Sigma-Aldrich) and dissolved in Dulbecco's phosphate-buffered saline (DPBS) for further use.

Fabrication of GelMA Hydrogels Encapsulating Cells and MNPs. The details of GelMA synthesis and prepolymer solution preparation can be found in the Supporting Information. Three groups of hydrogel samples were fabricated. One sample group was defined as a hydrogel array on a glass slide (20 mm × 20 mm) (Figure 1A). Hydrogel samples were prepared with a constant volume of prepolymer solution (192 μL). The surface area and number of gels, *i.e.*, 16, 64, 256 for gel sizes of 2 mm × 2 mm × 300 μm, 1 mm × 1 mm × 300 μm, and 500 μm × 500 μm × 300 μm, were varied in each sample group using different dimensions of a photomask array (Figure 1A).

To fabricate the microscale hydrogels, 250 μL of prepolymer solution was pipetted onto a flat polystyrene surface (Petri dish). The prepolymer solution was then covered by a 3-(trimethoxysilyl)propyl methacrylate (TMSPMA)-coated glass slide, which was separated from the Petri dish surface using two layers of glass slides (150 μm in thickness) as spacers with a total height of 300 μm. The photomask was then placed on the glass slide (Figure 1A). The prepolymer solution was exposed to UV light (360−480 nm) at 6.9 mW/cm^2 for 40 s to cross-link both MNP-encapsulating and MNP-free control hydrogels. The cover slide was removed and washed with DPBS to remove any excess prepolymer solution, resulting in a sample of gel array (Figure 1A). The samples were then placed into a six-well plate and cultured at 37 °C with 4 mL of 3T3 media (Figure 1B).

Mechanical Testing. To evaluate the effect of MNPs on the mechanical properties of the hydrogel, nonconfined compression tests were performed by using ADMET eXpert 2600 dual column testing machines (Norwood, MA, USA). To prepare the samples for the mechanical test, GelMA solution including photoinitiator was poured onto a flat surface (*e.g.*, Petri dish) and exposed to 6.9 mW/cm^2 UV light (360−480 nm) for 40 s. To test MNP related effects, prepolymer solutions containing 1% and 5% of MNP were used and all samples were allowed to swell in DPBS at room temperature for 24 h. Then, 12 mm of cylinder-shaped discs for each hydrogel sample (n = 5) was generated by using a biopsy punch. Hydrogel samples were compressed at a rate of 0.2 mm/min until failure occurred. The Young's modulus was determined as the slope of the initial linear region of the compressive stress−strain curve in the first 5−20% strain range.

Swelling Measurement. To analyze the swelling behavior of gels, we used prepolymer solution containing 1% and 5% MNPs. A 100 μL amount of prepolymer was pipetted between two glass coverslips separated by a 1 mm spacer and exposed to 6.9 mW/cm^2 UV light (360−480 nm) for 40 s. Then the cross-linked hydrogels were immersed in DPBS to swell at 37 °C for 24 h. Hydrogels were taken out of DPBS and blotted with a Kimwipe to remove the residual liquid. The swollen weight was recorded using a Mettler Toledo AB265 balance (Columbia, MD, USA). Samples (n = 16) were then lyophilized and weighed once more to determine the polymer dry weight. The mass swelling ratio was then calculated as the ratio of swollen hydrogel mass to the mass of dry polymer. All results were further analyzed by using ANOVA with Tukey's *posthoc* test.

***In Vitro* Enzymatic Degradation of Hydrogels.** To characterize the enzyme-mediated degradation of GelMA hydrogels (control), we fabricated gels with a size of 8 mm × 8 mm × 2 mm (GelMA 5% (w/v) and a photoinitiator concentration of 1% (w/v)) using a polydimethylsiloxane mold and cross-linked under UV conditions of 6.9 mW/cm^2 for 120 s. We measured the dry weight of the hydrogels. To investigate the effect of cells and MNPs on hydrogel degradation, four different hydrogel sample groups were fabricated: (1) GelMA hydrogel, (2) GelMA hydrogel encapsulating both cells and MNPs, (3) GelMA encapsulating only cells, (4) GelMA hydrogel encapsulating only MNPs. For the degradation analysis, 1% MNP concentration (w/v) and 1 × 10^6 cells/mL cell concentration were used. Fabricated hydrogels were cultured with 4 mL of 3T3 media with 2 U/mL collagenase type I (Figure 1B). At predefined time points (t = 12, 24, 36, 48, 60, 72, 84, 96 h), hydrogels were removed and lyophilized. The mass loss was determined as the ratio of the final dry weight to the original dry weight. The dry weight was measured using an analytical lab balance scale (Mettler Toledo, AB265-S/FACT). For each degradation experiment, we used 3−10 samples and reported mean and standard deviation.

Characterization of MNP Release Using ICP-AES. At intervals of 6 h after fabrication, the hydrogel samples in each well were imaged using an inverted microscope (Nikon T2000). Images were processed for hydrogel area change using the public domain NIH ImageJ program (http://rsb.info.nih.gov/nih-image/). At t = 6, 12, 18, 24, and 30 h, cell media in each well was collected and replaced by 4 mL of fresh 3T3 media containing 2 U/mL collagenase type I. To assess the MNP release, collected media samples were tested through ICP-AES for iron concentration. To prepare samples for ICP measurement, collected media samples were first heated to 70 °C using a standard benchtop hot plate (Corning, MA, USA) for 24 h to completely evaporate the collected medium. Then, each sample was added into 1 mL of 37% HCl and vortexed to allow complete dissolution of the MNPs into an ionic state. Samples were reheated again to 70 °C for 12 h to evaporate HCl. Finally, each sample was added into 3 mL of 2% nitric acid and filtered using a 0.2 μL surfactant-free cellulose acetate membrane filter (VWR Scientific) to remove any traces of organic matter and impurities.

Cell Culture and Cell Encapsulation. NIH 3T3 fibroblasts were used for cell viability and growth tests. The cells were cultured in DMEM supplemented with 10% FBS (Gibco) and 1% penicillin−streptomycin (Gibco) under standard cell culture conditions, *i.e.*, 37 °C, 95% humidity and 5% CO_2. When confluent, 3T3 fibroblasts were trypsinized and suspended in the prepared prepolymer solution at a cell concentration of 1 × 10^6 cells/mL.

Short-Term and Long-Term Cell Viability Test. The short-term (with collagenase type I) and long-term (without collagenase type I) cell viability in MNP-encapsulating hydrogels (1 mm × 1 mm × 300 μm) was assessed for two MNP concentrations (1% and 5%) (w/v). For the short-term and long-term viability assays, 5 × 10^6 and 1 × 10^6 cells/mL concentrations were used, respectively. The samples were cultured in 4 mL of 3T3 media with 2 U/mL collagenase type I (short-term) and without collagenase type I (long-term). Hydrogels were incubated with live/dead staining assay for 30 min. The live/dead dyes were prepared by diluting 2 μL of ethidium homodimer-1 and 0.5 μL of calcein (Molecullar Probes, Carlsbad, CA, USA) in 1 mL of DPBS. The fluorescence images were taken using a microscope (Nikon T2000). Images were processed using the NIH ImageJ program. Cell viability was characterized at t = 6, 12, and 24 h after hydrogel fabrication for the short-term test and at t = 24, 48, 72, 96, 120, and 144 h for the long-term test. Fluorescence images (Figure S3) were evaluated and the total cell numbers (sum of dead and live cells) at these time points were normalized to the total cell number at t = 24 h (*i.e.*, fold changes). A control with MNP-free hydrogels was used for the cell viability study.

Conflict of Interest: The authors declare no competing financial interest.

Acknowledgment. We would like to acknowledge NIH R21-HL112114 and R21-HL095960. U.D. acknowledges that this material is based in part upon work supported by the National Science Foundation under NSF CAREER Award Number 1150733. D.K. acknowledges support from The Scientific and Technological Research Council of Turkey. Any opinions, findings, and conclusions or recommendations expressed in this material are those of the author(s) and do not necessarily reflect the views of the National Science Foundation.

Supporting Information Available: The microstructure of hydrogels was analyzed using SEM. The details of sample preparation for SEM, imaging, and statistical analyses used in this study can be found. This material is available free of charge *via* the Internet at http://pubs.acs.org. F.X. and U.D. developed the idea; F.X., F.I., O.M., Y.S., D.K., B.Q.L., and U.D. designed the experimental approach; F.X., F.I., O.M., U.A.G., Y.S., D.K., B.Q.L., and U.D. performed the experiments; F.X., F.I., O.M., U.A.G., Y.S., D.K., B.Q.L., and U.D. analyzed the data; E.B.D. consulted on the manuscript; F.X., F. I., O.M., U.A.G., D.K., and U.D. wrote the manuscript.

REFERENCES AND NOTES

1. Hasirci, V.; Vrana, E.; Zorlutuna, P.; Ndreu, A.; Yilgor, P.; Basmanav, F. B.; Aydin, E. Nanobiomaterials: A Review of the Existing Science and Technology, and New Approaches. *J. Biomater. Sci., Polym. Ed.* **2006**, *17*, 1241–1268.
2. Xu, F.; Wu, C.-a. M.; Rengarajan, V.; Finley, T. D.; Keles, H. O.; Sung, Y.; Li, B.; Gurkan, U. A.; Demirci, U. Three-Dimensional Magnetic Assembly of Microscale Hydrogels. *Adv. Mater.* **2011**, *23*, 4254–4260.
3. Geckil, H.; Xu, F.; Zhang, X.; Moon, S.; Demirci, U. Engineering Hydrogels as Extracellular Matrix Mimics. *Nanomedicine (London, U. K.)* **2010**, *5*, 469–484.
4. Hung, H.-S.; Chen, H.-C.; Tsai, C.-H.; Lin, S.-Z. Novel Approach by Nanobiomaterials in Vascular Tissue Engineering. *Cell Transplant* **2011**, *20*, 63–70.
5. Miyahara, Y.; Kobayashi, H.; Chen, G.; Kikuchi, M. Focus on Nanobiomaterials and Technologies for Breakthrough in Future Medicine. *Sci. Technol. Adv. Mater.* **2010**, *11*, 010302.
6. Malvadkar, N. A.; Hancock, M. J.; Sekeroglu, K.; Dressick, W. J.; Demirel, M. C. An Engineered Anisotropic Nanofilm with Unidirectional Wetting Properties. *Nat. Mater.* **2010**, *9*, 1023–1028.
7. Stevens, M. M.; George, J. H. Exploring and Engineering the Cell Surface Interface. *Science* **2005**, *310*, 1135–1138.
8. Souza, G. R.; Molina, J. R.; Raphael, R. M.; Ozawa, M. G.; Stark, D. J.; Levin, C. S.; Bronk, L. F.; Ananta, J. S.; Mandelin, J.; Georgescu, M.-M.; *et al*. Three-Dimensional Tissue Culture Based on Magnetic Cell Levitation. *Nat. Nanotechnol.* **2010**, *5*, 291–296.
9. Dobson, J. Remote Control of Cellular Behaviour with Magnetic Nanoparticles. *Nat. Nanotechnol.* **2008**, *3*, 139–143.
10. Okochi, M.; Takano, S.; Isaji, Y.; Senga, T.; Hamaguchi, M.; Honda, H. Three-Dimensional Cell Culture Array using Magnetic Force-based Cell Patterning for Analysis of Invasive Capacity of BALB/3T3/v-src. *Lab Chip* **2009**, *9*, 3378–3384.
11. Gupta, A. K.; Curtis, A. S. Surface Modified Superparamagnetic Nanoparticles for Drug Delivery: Interaction Studies with Human Fibroblasts in Culture. *J. Mater. Sci.: Mater. Med.* **2004**, *15*, 493–496.
12. Kose, A. R.; Fischer, B.; Mao, L.; Koser, H. Label-free Cellular Manipulation and Sorting *via* Biocompatible Ferrofluids. *Proc. Natl. Acad. Sci. U. S. A.* **2009**, *106*, 21478–21483.
13. Krebs, M. D.; Erb, R. M.; Yellen, B. B.; Samanta, B.; Bajaj, A.; Rotello, V. M.; Alsberg, E. Formation of Ordered Cellular Structures in Suspension *via* Label-free Negative Magnetophoresis. *Nano Lett.* **2009**, *9*, 1812–1817.
14. Apple, F. S. Biomarkers in Aggregate. *Nat. Biotechnol.* **2011**, *29*, 236–237.
15. Laulicht, B.; Gidmark, N. J.; Tripathi, A.; Mathiowitz, E. Localization of Magnetic Pills. *Proc. Natl. Acad. Sci. U. S. A.* **2011**, *108*, 2252–2257.
16. Souza, G. R.; Christianson, D. R.; Staquicini, F. I.; Ozawa, M. G.; Snyder, E. Y.; Sidman, R. L.; Miller, J. H.; Arap, W.; Pasqualini, R. Networks of Gold Nanoparticles and Bacteriophage as Biological Sensors and Cell-targeting Agents. *Proc. Natl. Acad. Sci. U. S. A.* **2006**, *103*, 1215–1220.
17. Souza, G. R.; Yonel-Gumruk, E.; Fan, D.; Easley, J.; Rangel, R.; Guzman-Rojas, L.; Miller, J. H.; Arap, W.; Pasqualini, R. Bottom-Up Assembly of Hydrogels from Bacteriophage and Au Nanoparticles: The Effect of Cis- and Trans-Acting Factors. *Plos One* **2008**, *3*, e2242.
18. Hwang, D. K.; Dendukuri, D.; Doyle, P. S. Microfluidic-based Synthesis of Non-spherical Magnetic Hydrogel Microparticles. *Lab Chip* **2008**, *8*, 1640–1647.
19. Chen, C.-H.; Abate, A. R.; Lee, D.; Terentjev, E. M.; Weitz, D. A. Microfluidic Assembly of Magnetic Hydrogel Particles with Uniformly Anisotropic Structure. *Adv. Mater.* **2009**, *21*, 3201–3204.
20. Yuet, K. P.; Hwang, D. K.; Haghgooie, R.; Doyle, P. S. Multifunctional Superparamagnetic Janus Particles. *Langmuir* **2009**, *26*, 4281–4287.
21. Lee, H.; Kim, J.; Kim, H.; Kwon, S. Colour-barcoded Magnetic Microparticles for Multiplexed Bioassays. *Nat. Mater.* **2010**, *9*, 745–749.
22. Bong, K. W.; Chapin, S. C.; Doyle, P. S. Magnetic Barcoded Hydrogel Microparticles for Multiplexed Detection. *Langmuir* **2010**, *26*, 8008–8014.
23. Zhao, X.; Kim, J.; Cezar, C. A.; Huebsch, N.; Lee, K.; Bouhadir, K.; Mooney, D. J. Active Scaffolds for on-demand Drug and Cell Delivery. *Proc. Natl. Acad. Sci. U. S. A.* **2011**, *108*, 67–72.
24. Xu, F.; Moon, S. J.; Emre, A. E.; Turali, E. S.; Song, Y. S.; Hacking, S. A.; Nagatomi, J.; Demirci, U. A Droplet-based Building Block Approach for Bladder Smooth Muscle Cell (SMC) Proliferation. *Biofabrication* **2010**, *2*, 014105.
25. Moon, S.; Hasan, S. K.; Song, Y. S.; Xu, F.; Keles, H. O.; Manzur, F.; Mikkilineni, S.; Hong, J. W.; Nagatomi, J.; Haeggstrom, E.; *et al*. Layer by Layer Three-Dimensional Tissue Epitaxy by Cell-Laden Hydrogel Droplets. *Tissue Eng., Part C* **2010**, *16*, 157–166.
26. LaConte, L.; Nitin, N.; Bao, G. Magnetic Nanoparticle Probes. *Mater. Today* **2005**, *8*, 32–38.
27. Ito, A.; Ino, K.; Kobayashi, T.; Honda, H. The Effect of RGD Peptide-conjugated Magnetite Cationic Liposomes on Cell Growth and Cell Sheet Harvesting. *Biomaterials* **2005**, *26*, 6185–6193.
28. Hautot, D.; Pankhurst, Q. A.; Morris, C. M.; Curtis, A.; Burn, J.; Dobson, J. Preliminary Observation of Elevated Levels of Nanocrystalline Iron Oxide in the Basal Ganglia of Neuroferritinopathy Patients. *Biochim. Biophys. Acta* **2007**, *1772*, 21–25.
29. Shubayev, V. I.; Pisanic, T. R., II; Jin, S. Magnetic Nanoparticles for Theragnostics. *Adv. Drug Delivery Rev.* **2009**, *61*, 467–477.
30. Lanone, S.; Boczkowski, J. Biomedical Applications and Potential Health Risks of Nanomaterials: Molecular Mechanisms. *Curr. Mol. Med.* **2006**, *6*, 651–663.
31. Hafeli, U. O.; Riffle, J. S.; Harris-Shekhawat, L.; Carmichael-Baranauskas, A.; Mark, F.; Dailey, J. P.; Bardenstein, D. Cell Uptake and *in Vitro* Toxicity of Magnetic Nanoparticles Suitable for Drug Delivery. *Mol. Pharm.* **2009**, *6*, 1417–1428.
32. Berry, C. C.; Wells, S.; Charles, S.; Curtis, A. S. Dextran and Albumin Derivatised Iron Oxide Nanoparticles: Influence on Fibroblasts *in Vitro*. *Biomaterials* **2003**, *24*, 4551–4557.
33. Nicodemus, G. D.; Bryant, S. J. Cell Encapsulation in Biodegradable Hydrogels for Tissue Engineering Applications. *Tissue Eng. Part B* **2008**, *14*, 149–165.
34. Tan, H.; Marra, K. G. Injectable, Biodegradable Hydrogels for Tissue Engineering Applications. *Materials* **2010**, *3*, 1746–1767.
35. Hunt, N. C.; Smith, A. M.; Gbureck, U.; Shelton, R. M.; Grover, L. M. Encapsulation of Fibroblasts Causes Accelerated Alginate Hydrogel Degradation. *Acta Biomater.* **2010**, *6*, 3649–3656.
36. Bedard, M. F.; Munoz-Javier, A.; Mueller, R.; del Pino, P.; Fery, A.; Parak, W. J.; Skirtach, A. G.; Sukhorukov, G. B. On the Mechanical Stability of Polymeric Microcontainers Functionalized with Nanoparticles. *Soft Matter* **2009**, *5*, 148–155.
37. Kolesnikova, T. A.; Gorin, D. A.; Fernandes, P.; Kessel, S.; Khomutov, G. B.; Fery, A.; Shchukin, D. G.; Moehwald, H. Nanocomposite Microcontainers with High Ultrasound Sensitivity. *Adv. Funct. Mater.* **2010**, *20*, 1189–1195.
38. Gil, E. S.; Frankowski, D. J.; Spontak, R. J.; Hudson, S. M. Swelling Behavior and Morphological Evolution of Mixed Gelatin/Silk Fibroin Hydrogels. *Biomacromolecules* **2005**, *6*, 3079–3087.
39. Wang, Y.; Li, B.; Zhou, Y.; Jia, D. Chitosan-induced Synthesis of Magnetite Nanoparticles *via* Iron Ions Assembly. *Polym. Adv. Technol.* **2008**, *19*, 1256–1261.
40. Xia, H.-B.; Yi, J.; Foo, P.-S.; Liu, B. Facile Fabrication of Water-Soluble Magnetic Nanoparticles and Their Spherical Aggregates. *Chem. Mater.* **2007**, *19*, 4087–4091.
41. Balazs, A. C.; Emrick, T.; Russell, T. P. Nanoparticle Polymer Composites: Where Two Small Worlds Meet. *Science* **2006**, *314*, 1107–1110.
42. Han, J. H.; Lee, E. J.; Lee, J. H.; So, K. P.; Lee, Y. H.; Bae, G. N.; Lee, S. B.; Ji, J. H.; Cho, M. H.; Yu, I. J. Monitoring Multiwalled Carbon Nanotube Exposure in Carbon Nanotube Research Facility. *Inhalation Toxicol.* **2008**, *20*, 741–749.

43. Tsai, S. J.; Hofmann, M.; Hallock, M.; Ada, E.; Kong, J.; Ellenbecker, M. Characterization and Evaluation of Nanoparticle Release During the Synthesis of Single-walled and Multiwalled Carbon Nanotubes by Chemical Vapor Deposition. *Environ. Sci. Technol.* **2009**, *43*, 6017–6023.
44. Kaegi, R.; Ulrich, A.; Sinnet, B.; Vonbank, R.; Wichser, A.; Zuleeg, S.; Simmler, H.; Brunner, S.; Vonmont, H.; Burkhardt, M.; *et al*. Synthetic TiO_2 Nanoparticle Emission from Exterior Facades into the Aquatic Environment. *Environ. Pollut.* **2008**, *156*, 233–239.
45. Tsai, S.-J.; Ada, E.; Isaacs, J. A.; Ellenbecker, M. J. Airborne Nanoparticle Exposures Associated with the Manual Handling of Nanoalumina and Nanosilver in Fume Hoods. *J. Nanopart. Res.* **2009**, *11*, 147–161.
46. Verberg, R.; Alexeev, A.; Balazs, A. C. Modeling the Release of Nanoparticles from Mobile Microcapsules. *J. Chem. Phys.* **2006**, *125*, 224712.
47. Yeo, Y.; Ito, T.; Bellas, E.; Highley, C. B.; Marini, R.; Kohane, D. S. *In Situ* Cross-linkable Hyaluronan Hydrogels containing Polymeric Nanoparticles for Preventing Postsurgical Adhesions. *Ann. Surg.* **2007**, *245*, 819–824.
48. Hu, J.; Hiwatashi, K.; Kurokawa, T.; Liang, S. M.; Wu, Z. L.; Gong, J. P. Microgel-Reinforced Hydrogel Films with High Mechanical Strength and Their Visible Mesoscale Fracture Structure. *Macromolecules* **2011**, *44*, 7775–7781.
49. Tokatlian, T.; Shrum, C. T.; Kadoya, W. M.; Segura, T. Protease Degradable Tethers for Controlled and Cell-Mediated Release of Nanoparticles in 2- and 3-Dimensions. *Biomaterials* **2010**, *31*, 8072–8080.